# Tuning from frustrated magnetism to superconductivity in quasi-one-dimensional KCr_{3}As_{3} through hydrogen doping

Keith M. Taddei, Liurukara D. Sanjeewa, Bing-Hua Lei, Yuhao Fu, Qiang Zheng, David J. Singh, Athena S. Sefat, and Clarina dela Cruz

Phys. Rev. B **100**, 220503 — Published 16 December 2019

DOI: 10.1103/PhysRevB.100.220503

# Tuning from Frustrated Magnetism to Superconductivity in Quasi-One-Dimensional $KCr_3As_3$ Through Hydrogen Doping

Keith M. Taddei,[1,*] Liurukara D. Sanjeewa,[2] Bing-Hua Lei,[3] Yuhao Fu,[3]
Qiang Zheng,[2] David J. Singh,[3] Athena S. Sefat,[2] and Clarina dela Cruz[1]

[1] *Neutron Scattering Division, Oak Ridge National Laboratory, Oak Ridge, TN 37831*
[2] *Materials Science and Technology Division, Oak Ridge National Laboratory, Oak Ridge, TN 37831*
[3] *Department of Physics and Astronomy, University of Missouri, Missouri 65211, USA*

(Dated: December 2, 2019)

We report the charge doping of $KCr_3As_3$ via H intercalation. We show that the previously reported ethanol bath deintercalation of $K_2Cr_3As_3$ to $KCr_3As_3$ has a secondary effect whereby H from the bath enters the quasi-one-dimensional $Cr_6As_6$ chains. Furthermore, we find that - contrary to previous interpretations - the difference between non-superconducting as-grown $KCr_3As_3$ samples and superconducting hydrothermally annealed samples is not a change in crystallinity but due to charge doping with the latter treatment increasing the H concentration in the CrAs tubes effectively electron-doping the 133 compound. These results suggest a new stoichiometry $KH_xCr_3As_3$, that superconductivity arises from a suppressed magnetic order via a tunable parameter and paves the way for the first charge-doped phase diagram in these materials.

PACS numbers: 74.25.Dw, 74.62.Dh, 74.70.Xa, 61.05.fm

Arguably the start of quantum materials, superconductors have suggested topological classifications, given rise to the Resonating Valence Bond theory used in quantum spin-liquids and form the basis of numerous technologies in quantum information [1–6]. Yet unlike many of the topological quantum materials whose physics are understood but which struggle to find physical realizations, unconventional superconductors exist but have no settled microscopic theory leaving their optimization unguided [3, 7–10]. Instead, we rely on an empirical recipe derived of a surprisingly universal phase diagram where superconductivity is found near instabilities [11].

To refine this recipe and discriminate between possible mechanisms, it is useful to find new unconventional superconductors which are structurally simple, have few orders and are easy to address theoretically (e.g. fewer relevant orbitals, lower dimensionality.) Much as the iron superconductors helped refine themes from the cuprates, a new family of superconductors $A_2TM_3As_3$ ($A$ = Na, K, Cs or Rb, $TM$ = Cr or Mo and $P\bar{6}m2$ symmetry) has begun offering insights, but helpfully via a quasi-one-dimensional structure [11–17]. Neutron scattering, nuclear magnetic resonance, Raman scattering and density functional theory work have revealed both structural and magnetic instabilities - as seen in the iron-based superconductors [18–23]. However, in $K_2Cr_3As_3$ for instance these orders break different symmetries, show no coupling, and suggest that only magnetism couples to superconductivity [18, 19]. Additionally, evidence of Luttinger liquid physics, spin-triplet superconductivity, topological superconductivity and a nodal gap function have emerged indicating the broader novelty of this system [24–31]. Nonetheless, its study has been inhibited by an extreme air sensitivity and lack of charge doped variants [32].

Promisingly, $KCr_3As_3$ (with $P6_3/m$ symmetry) addresses these issues with both a diminished electron count and stability in air. $KCr_3As_3$ (or '133' as opposed to '233' for $K_2Cr_3As_3$) is created by soaking 233 in ethanol which ostensibly, removes one K while retaining the quasi-one dimensional CrAs tubes and thus affords access to end-members of a potential phase diagram [33]. Yet, results from $KCr_3As_3$ (and the broader $ACr_3As_3$ family) have proven contentious. Initially it was reported as non-superconduting with spin-glass like magnetism [16, 33]. More recently a post-bath hydrothermal ethanol anneal was found to produce bulk superconductivity with non-magnetic behavior [34, 35]. Similarly, theory work has found conflict, with reports of long range magnetic ground states, Fermi-surface nesting mediated superconductivity and of a structural instability which precludes spin-mediated superconductivity [31, 36, 37].

Previously, crystalline disorder has been suggested to explan these conflicting results - in Ref. 34 it is argued that superconductivity arises in $KCr_3As_3$ upon post-annealing due to an improvement of the crystallinity. While in theory work, Ref. 36 suggests its predicted mag-

netic order is not seen experimentally due to disorder in the physical material and Ref. 37 suggests that similar to $K_2Cr_3As_3$ the predicted structural instability may have no long range coherence [19]. In attempting to sort through these possibilities, we stumbled upon an unexpected but useful origin to these discrepancies.

Here we report a systematic study of synthesis reactions for $KCr_3As_3$ using neutron and x-ray diffraction together with Density Functional Theory (DFT). We reveal a previously missed effect of the ethanol bath whereby H is unavoidably intercalated into the CrAs tubes leading to a $KH_xCr_3As_3$ stoichiometry. We show that H concentration is controllable and that the difference between non-superconducting spin-glass and non-magnetic superconducting samples is not in the sample crystallinity but in the amount of H intercalated. Our DFT work suggests that the $KH_xCr_3As_3$ structure is stable, electron-doped relative to $KCr_3As_3$ and exhibits an electronic structure more similar to $K_2Cr_3As_3$ than $KCr_3As_3$. Additionally, we find that the H stabilizes the $P6_3/m$ structure and places the compound proximate to an antiferromagnetic instability. These results lead to the exciting possibility of continuously tuning $KH_xCr_3As_3$ from a spin-glass to a superconductor via charge doping with H - the long sought after tuning parameter. Furthermore this shifts interest to a new air stable compound opening up this system for widespread study. More contemplatively, it offers a realization of a frustrated magnetic to superconducting transition in a quasi-one-dimensional (Q1D) system which has long been suggested as a potential recipe for spin liquid physics [38, 39].

Neutron powder diffraction (NPD) data were collected using the HB-2A and NOMAD diffractometers of Oak Ridge National Laboratory's High Flux Isotope Reactor and Spallation Neutron Source [40–42]. High resolution synchrotron x-ray powder diffraction (XRD) data were collected at beamline 11BM-B of the Advanced Photon Source at Argonne National Laboratory. Structural analysis was performed using the Rietveld method as implemented in the FullProf, GSAS and EXPGUI software suites (see Supplemental Materials (SM) 43 for more details) [44–47]. DFT calculations were performed using projector-augmented plane-wave method and checked using the general potential linearized augmented planewave method as implemented in VASP and WIEN2k respectively [48–52]. Phonon spectrums were calculated using the PHONOPY code [53]. For more details on the calculations see the SM 43 and references contained therein 54.

To study how the synthesis procedures effect the measured propetries, we synthesized powder samples following the methodologies reported by Bao *et al.,* in Ref. 33 and Mu *et al.,* in Ref. 34. Thus three samples were used for initial characterization: (S1) as grown from an ethanol bath, (S2) with a post-bath vacuum anneal and (S3) with both post-bath hydrothermal and vacuum anneals (a fourth sample (S4) was also grown and will be discussed later in this text). Susceptibility measurements show we were successful in reproducing the previously reported change in properties with S1 and S2 being trace-superconductors with spin-glass properties (identified here as in Ref. 33) and S3 showing bulk superconductivity (see SM 43).

Previously, the change in properties was attributed to the post-bath annealings' effects on the crystallinity of the sample. Ostensibly, the more crystalline annealed samples hosted superconductivity which was otherwise destroyed by disorder in the as-grown samples [34]. To test this assertion NPD and XRD data were collected and are shown along with the best fit results of Rietveld refinements in Fig. 1. We note that even visually, the main qualitative difference between the samples is not in the peak shape but in the background to signal ratio. Specifically, in the NPD data the bulk superconducting S3 has a remarkably larger background to signal ratio than any other sample.

To qualitatively check the crystallographic properties, the NPD and XRD were used together for Rietveld refinements. From this analysis, the lattice parameters and measures of strain, crystallinity and grain size can be assessed (plotted as a function of sample number along with the 233 compound labeled as sample 5 in Fig. 2). Considering the extracted anisotropic microscopic strain parameters ($L_{nn}$ where $n = 1, 2, 3$ correspond to the $a, b$ and $c$ lattice directions respectively) and $L_x$ (which is proportional to the inverse of the crystallite size), little difference is seen in these terms between samples indicating similar crystalline properties. Compared to the broadening parameters determined in previous work on the 233 compound (Ref. 18), it is seen that generally the deintercalation process leaves the 133 material with poor crystallinity. However, it is not significantly improved upon either vacuum or hydrothermal annealing, in contrast with previous reports which did not compare qualitative measures of the crystallinity [34].

Looking at the crystal parameters a clear trend relative to the superconducting volume fraction is seen (Fig. 2 (b)). Both the $a$ and $c$ lattice parameters dilate between the trace (S2) and bulk (S3) superconducting samples by 0.1 and 0.4 % respectively leading to a $> 0.4$ % change in the unit cell volume (Fig. 2 (b)). On the other hand, between S1 and S2 no such change is seen with only a small $\sim 0.1$ % change in volume. These results are unexpected: if the post-annealing treatments improve the crystallinity the peak broadening terms should decrease and the unit cell relax - our data directly contradict this [55, 56]. Therefore, we searched for a different explaination for the change in properties between the trace and bulk superconducting samples.

Noting that the background to signal increase is only seen in NPD and is exacerbated by the hydrothermal anneal, we posit the presence of H in the samples. H is

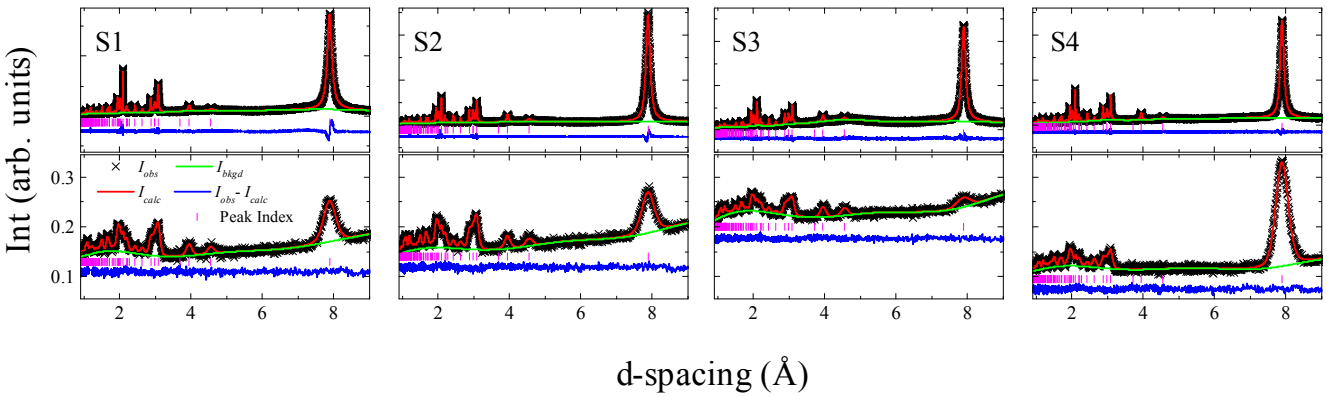


FIG. 1. Room temperature x-ray (top row) and neutron (bottom row) powder diffraction patterns for the four $KCr_3As_3$ samples plotted with the results of Rietveld refinements for H and D containing models. The neutron diffraction data was collected using identical sample mass, neutron exposures and sample containers and are thus the scattered neutron intensity is directly comparable between samples.

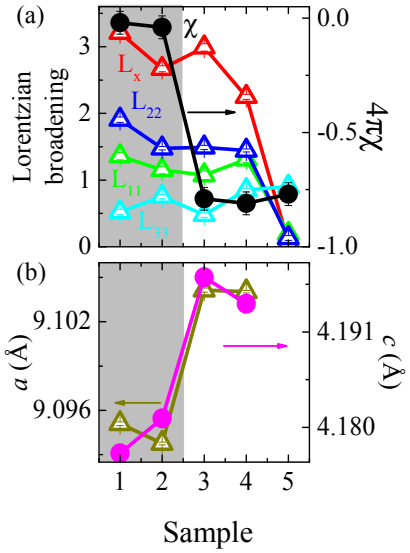


FIG. 2. (a) Lorentzian broadening terms in the GSAS profile fitting function including three terms for micro-strain along the unit cell directions ($L_{11}$, $L_{22}$ and $L_{33}$) and one term ($L_x$) for particle size broadening. This latter is proportional to the inverse of the particle size. The superconducting volume fraction determined at 1.5 K is over-plotted with sample 5 denoting the pure 233 compound. (b) the refined $a$ and $c$ lattice parameters. Throughout the figure data with scale on the left axis are plotted with open triangles while data with scale on the right axis are plotted as filled circles. The grey shaded region denotes samples with only trace superconductivity.

nearly invisible to x-rays but has a large incoherent cross-section to neutrons ($\sigma_{H_{Inc}} \sim 80.26\ b$) [57]. This manifests as a large background which increases with d-spacing and could explain the difference between the XRD and NPD patterns [58]. As such, any H in $KCr_3As_3$ would be missed in XRD and energy dispersive x-ray spectroscopy elucidating why such a feature has not been seen in previous structural work [16, 33–35]. We propose several mechanisms which would introduce H to the samples during the ethanol baths: a remnant minority organic compound not removed during washing, substitution onto the K site or intercalation into the 133 structure. Of these scenarios the latter two provide an explanation for the increase in background upon the hydrothermal anneal assuming the process either forces more H into the material through higher temperature, pressure or a longer exposure to ethanol.

To discriminate between these scenarios, a sample of 133 was grown following the procedure of S3 but using fully deuterated ethanol in all steps. The resulting sample (S4) shows simlar superconducting properties to S3 (see SM 43) indicating that the use of deuterated ethanol does not significantly change the sample properties. Deuterium (D) does not have the large incoherent cross section of H ($\sigma_{D_{Inc}} \sim 2.05\ b$) and so does not add as much background scattering. Furthermore, it has a large coherent cross-section ($\sigma_{D_{Coh}} \sim 7.6\ b$) allowing for reliable structural model refinements (the coherent cross-sections of K, Cr, As and H are 1.69, 1.66, 5.44 and 1.76 $b$ respectively) [57]. Therefore, if H is intercalated or substitutes for K using D would allow for structure solution and composition determination through changes in peak intensities, else if the H background comes from remnant organic compounds the background will be reduced in S4 but no other changes should occur.

The XRD and NPD of S4 are shown in Fig. 1. While the XRD looks similar to the other samples, the NPD exhibits a nearly 50% reduction in background (compared to S3) as well as a change in peak intensities where peaks at 3.9 and 4.6 Å (the (020) and (110) reflections respectively) become background equivalent. The background reduction confirms the presence of H in the samples (rather than for instance the background arising from amorphous parts of the sample) while the change in

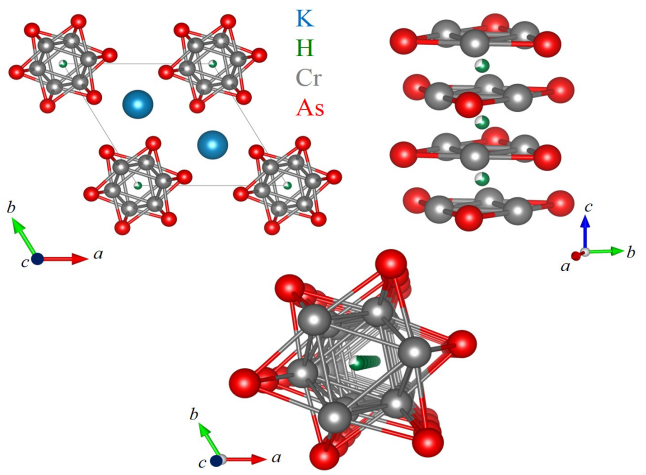


FIG. 3. $KH_xCr_3As_3$ structure as viewed along the $c$-axis, perpendicular to the $c$-axis and along the CrAs tubes. K, H, Cr and As atoms are denoted by turquoise, dark green, gray and red spheres respectively. The partial occupancy of the H site is indicated by a wedge of white in the H atom surface.

peak intensities indicates that the H and D are incorporated into the 133's crystal structure rather than existing as remnant organic compounds.

To determine where D is incorporated, Rietveld analysis was performed using the NPD. Since the D containing sample shows a reduction in peak intensity but not the appearance of new peaks the original $P6_3/m$ crystal symmetry was used and Rietveld refinements were performed trying models containing D on all of $P6_3/m$'s special Wyckoff positions. Of these, only models with D on the 2$b$ (0,0,0) site reproduced the observed intensities as shown in Fig. 1 leading to high quality fits with small residuals (see SM for fit parameters 43).

The new structural model is shown in Fig. 3. In it, D is intercalated into the center of the CrAs tubes between the stacked CrAs layers creating a chain of D centered in each tube. We find no evidence of K vacancies or of D substitution on the K site. However, our refinements show the D site is only partially occupied with a refined occupancy of 65% .

With the location in hand, Rietveld refinements were tried using similar models for S1, S2 and S3, this is possible since H has a coherent cross-section which is on the order of both K and Cr. Starting with S3, our refinements show agreement with S4, with a similar occupancy of $\sim 71$ % . This corroborates that the synthesis procedure and resulting material is insensitive to the change from H to D. On the other hand, S1 and S2 are found to have significantly less H than S3 and S4. Both the S1 and S2 models refine to have $\sim 35$ % H. As all samples show intercalated H - even the non-bulk superconductors - we revise the chemical formula of $KCr_3As_3$ to $KH_xCr_3As_3$ explicitly reflecting the H content and its variability.

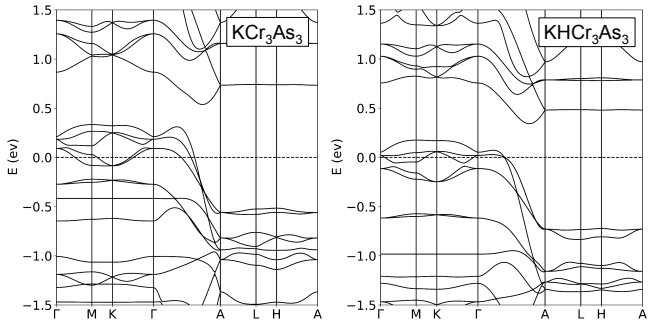


FIG. 4. DFT calculated band structure for (left) the $KCr_3As_3$ and (right) $KHCr_3As_3$ stoichiometries.

These results elucidate the effects of the different reaction stages. During the room temperature bath, K is deintercalated from the 233 starting material as reported previously however, some H from the bath also intercalates into the CrAs tubes between the CrAs layers. Whether this occurs to charge compensate for the deintercalated K is not known and should be the interest of future work - although this may be indicated by the inability to synthesize $KCr_3As_3$ directly from solid state methods [33, 34]. The similarities both in crystallinity and H content of S1 and S2 suggest that vacuum annealing neither improves the sample quality nor vents the intercalated H. This latter result suggests the stability of $KH_xCr_3As_3$ at least up to the annealing temperatures used in this work. Upon the hydrothermal annealing, more H intercalates into the structure bringing the concentration from $\sim 35$ to $\sim 65-71$ %.

It is this latter effect which appears to induce superconductivity in $KH_xCr_3As_3$. As discussed no change in crystallinity is seen between bulk and trace superconducting samples but rather a previously unexplained change in the lattice parameters. We can now ascribe this to an increase in the amount of H intercalated into the CrAs tubes. Beyond causing the unit cell to expand, the intercalated H should also affect the charge count however, the chemistry of H is incredibly flexible and its electronic contribution is not evident from the diffraction data [59, 60].

To study $KH_xCr_3As_3$'s energetics and electronic structure, DFT calculations were performed using the theoretical $x = 0$ and $x = 1$ stoichiometries. Calculations for $KHCr_3As_3$'s formation energy relative to $KCr_3As_3$ and $H_2$ gas found a negative formation energy of 92 kJ/mol $H_2$ - similar to that of other stable hydrides such as $MgH_2$ - indicating the intercalated structure is energetically favorable (see SM for more details) [43]. Calculations of $KHCr_3As_3$'s band structure (Fig. 4) show that the intercalated H raises the Fermi energy ($E_F$)and causes only modest distortions to the bands near $E_F$. Therefore, we can say that in $KHCr_3As_3$, H has metallic bonding and acts as an electron donor. As shown, it increases the electron count such that the electronic structure (and Fermi

surface see SM 43) are more similar to $K_2Cr_3As_3$ than the pure $KCr_3As_3$ suggesting similar electronic behavior.

Inspired by previous reports of instabilities, we also performed calculations of the phonon spectrum and proximity to magnetic instabilities [31, 36, 37, 61]. Considering the predicted structural instability, our calculations show no unstable phonon modes and relatively high energy nearly dispersionless H modes, suggesting that H removes the phonon instability leaving $KHCr_3As_3$ structurally stable [62]. Finally, we consider the hydride's proximity to magnetic instabilities. Previously, $KCr_3As_3$ has been suggested to either have a magnetic ground state which is frustrated by disorder, or no magnetic ground state due to a structural instability which removes favorable nesting conditions [36, 37]. For $KHCr_3As_3$ we find weak itinerant instabilities to both ferromagnetic and antiferromagnetic A-type magnetic orders with a slight preference for the latter. However, we also find both itinerancy and low energy scales suggesting that the magnetic order could easily be suppressed to a paramagnetic state with spin-fluctuations by quantum fluctuations such as the case of $Ni_3Ga$ [63]. This last result is quite interesting as it restores the possibility of a spin-driven pairing mechanism which had previously been discounted in Ref. 37.

These combined results suggest that superconductivity arises in $KH_xCr_3As_3$ upon electron doping, a process which until now has been achieved unintentionally during the hydrothermal anneal. In this scenario, the underdoped $KH_{0.35}Cr_3As_3$ is a non-superconducting spin-glass phase as reported by Bao. *et al.* [33]. Upon electron doping to $KH_{0.65}Cr_3As_3$ via hydrothermal annealing, the spin-glass phase is suppressed and the material becomes a bulk superconductor with $T_c \sim 5$ K as reported by Mu *et al.,* [34]. This has multiple significant implications: (i) the intercalated CrAs systems inhabit a familiar phase space where superconductivity arises out of a suppressed magnetic state, (ii) the possibility of creating the previously elusive charge doped phase diagram for the intercalated CrAs ($KH_xCr_3As_3$ as well as the Rb and Cs analogues), (iii) the need to revisit previous *ab initio* calculations on the $ACr_3As_3$ materials which were based on the hydrogen free 133 stoichiometry, (iv) an avenue to study how superconductivity arises from a frustrated magnetic state in a quasi-one-dimensional system by charge doping a concept which has long held interest for spin- and Luttinger liquid physics [38, 39]. As an additional point of interest, one of the significant impediments to the study of the intercalated CrAs materials to this point has been the 233 stoichiometry's extreme air sensitivity, with this work, we show a clear path forward to study interactions between magnetic and superconducting orders in the air stable 133 stoichiometry alleviating this barrier. Our results layout a rich path of future work, not least of which will be to gain fine control of the H content through the synthesis procedures.

*Note Added.* Over the course of the review process the authors are aware of two papers that have been published which further encourage work towards a $KH_xCr_3As_3$ phase diagram. One describes the complex chemistry leading to the H intercalation [64] while the other examines the calculated band structures of the system with and without H to predict the existence of a Lifshitz transition at some critical H concentration [64].

The part of the research conducted at ORNLs High Flux Isotope Reactor and Spallation Neutron Source was sponsored by the Scientific User Facilities Division, Office of Basic Energy Sciences (BES), U.S. Department of Energy (DOE). The research is partly supported by the U.S. DOE, BES, Materials Science and Engineering Division. Work at the University of Missouri is supported by the U.S. DOE, BES, Award No. DE-SC0019114. The authors thank J. Neuefeind and J. Liu for help with data collection on NOMAD.

* corresponding author taddeikm@ornl.gov

[1] J. Bednorz and K. Müller, Zeitschrift für Physik B Condensed Matter **64**, 189 (1986).
[2] P. Anderson, Science **235**, 1196 (1987).
[3] X.-G. Wen, Rev. Mod. Phys. **89**, 041004 (2017).
[4] Y. Nakamura, Y. Pashkin, and J. Tsai, Nature **398**, 786 (1999).
[5] N. Read and D. Green, Phys. Rev. B **61**, 10267 (2000).
[6] J. Linder and J. Robinson, Nat. Phys. **11**, 307 (2015).
[7] R. Fernandes and A. Chubukov, Reports on Progress in Physics **80**, 014503 (2016).
[8] S. Lee, P. Sharma, A. Lima-Sharma, W. Pan, and T. Nenoff, Chemistry of Materials **31**, 26 (2019).
[9] L. Balents, Nature **464**, 199 (2010).
[10] M. R. Norman, Science **332**, 196 (2011).
[11] D. Basov and A. Chubukov, Nat. Phys. **7**, 272 (2011).
[12] J. M. Allred, K. M. Taddei, D. E. Bugaris, M. J. Krogstad, S. H. Lapidus, D. Y. Chung, H. Claus, M. Kanatzidis, D. Brown, J. Kang, R. Fernandes, I. Eremin, S. Rosenkranz, O. Chmaissem, and R. Osborn, Nature Physics (2016), 10.1038/nphys3629.
[13] J.-K. Bao, J.-Y. Liu, C.-W. Ma, Z.-H. Meng, Z.-T. Tang, Y.-L. Sun, H.-F. Zhai, H. Jiang, H. Bai, C.-M. Feng, Z.-A. Xu, and G.-H. Cao, Physical Review X **5**, 011013 (2015).
[14] Q.-G. Mu, B.-B. Ruan, B.-J. Pan, T. Liu, J. Yu, K. Zhao, G.-F. Chen, and Z.-A. Ren, Phys. Rev. Mater. **2**, 034803 (2018).
[15] Q.-G. Mu, B.-B. Ruan, K. Zhao, B.-J. Pan, T. Liu, L. Shan, G.-F. Chen, and Z.-A. Ren, Science Bulletin **63**, 952 (2018).
[16] Z.-T. Tang, J. Bao, Y. Liu, H. Bai, H. Jiang, H.-F. Zhai, C.-M. Feng, Z.-A. Xu, and G.-H. Cao, Science China Materials **58**, 543 (2015).
[17] K. Zhao, Q.-G. Mu, T. Liu, B.-J. Pan, B.-B. Ruan, L. Shan, G.-F. Chen, and Z.-A. Ren, arXiv:1805.11577 (2018).
[18] K. M. Taddei, Q. Zheng, A. S. Sefat, and C. de la Cruz, Phys. Rev. B **96**, 180506 (2017).

[19] K. Taddei, G. Xing, J. Sun, Y. Fu, Y. Li, Q. Zheng, A. Sefat, D. Singh, and C. de la Cruz, Phys. Rev. Lett. **121**, 187002 (2018).

[20] H. Zhi, T. Imai, F. L. Ning, J.-K. Bao, and G.-H. Cao, Phys. Rev. Lett. **114**, 147004 (2015).

[21] W.-L. Zhang, H. Li, D. Xia, H. W. Liu, Y.-G. Shi, J. L. Luo, J. Hu, P. Richard, and H. Ding, Phys. Rev. B **92**, 060502 (2015).

[22] X.-X. Wu, C.-C. Le, J. Yuan, H. Fan, and J.-P. Hu, Chin. Phys. Lett. **32**, 057401 (2015).

[23] H. Jiang, G. Cao, and C. Cao, Sci. Rep. **5**, 16054 (2015).

[24] M. D. Watson, Y. Feng, C. W. Nicholson, C. Monney, J. M. Riley, H. Iwasawa, K. Refson, V. Sacksteder, D. T. Adroja, J. Zhao, and M. Hoesch, Phys. Rev. Lett. **118**, 097002 (2017).

[25] Y. Shao, X. Wu, L. Wang, Y. Shi, J. Hu, and J. Luo, EPL (Europhysics Letters) **123**, 57001 (2018).

[26] Y. Liu, J.-K. Bao, H.-K. Zuo, A. Ablimit, Z.-T. Tang, C.-M. Feng, Z.-W. Zhu, and G.-H. Cao, Sci. China: Phys., Mech. Astron. **59**, 657402 (2016).

[27] D. T. Adroja, A. Bhattacharyya, M. Telling, Y. Feng, M. Smidman, B. Pan, J. Zhao, A. D. Hillier, F. L. Pratt, and A. M. Strydom, Phys. Rev. B **92**, 134505 (2015).

[28] J. Sun, Y. Jiao, C. Yang, W. Wu, C. Yi, B. Wang, Y. Shi, J. Luo, Y. Uwatoko, and J. Cheng, Journal of Physics: Condensed Matter **29**, 455603 (2017).

[29] S.-M. Huang, C.-H. Hsu, S.-Y. Xu, C.-C. Lee, S.-Y. Shiau, H. Lin, and A. Bansil, Phys. Rev. B **97**, 014510 (2018).

[30] J. Yang, Z. T. Tang, G. H. Cao, and G.-q. Zheng, Physical Review Letters **115**, 147002 (2015).

[31] L.-D. Zhang, X. Zhang, J.-J. Hao, W. Huang, and F. Yang, Phys. Rev. B **99**, 094511 (2019).

[32] Q. Mu, B. Ruan, B. Pan, T. Liu, K. Zhao, G. Chen, and Z. Ren, Journal of Physics: Condensed Matter **31**, 225701 (2019).

[33] J.-K. Bao, L. Li, Z.-T. Tang, Y. Liu, Y.-K. Li, H. Bai, C.-M. Feng, Z.-A. Xu, and G.-H. Cao, Phys. Rev. B **91**, 180404 (2015).

[34] Q.-G. Mu, B.-B. Ruan, B.-J. Pan, T. Liu, J. Yu, K. Zhao, G.-F. Chen, and Z.-A. Ren, Phys. Rev. B **96**, 140504 (2017).

[35] T. Liu, Q.-G. Mu, B.-J. Pan, J. Yu, B.-B. Ruan, K. Zhao, G.-F. Chen, and Z.-A. Ren, EPL (Europhysics Letters) **120**, 27006 (2017).

[36] C. Cao, H. Jiang, X.-Y. Feng, and J. Dai, Phys. Rev. B **92**, 235107 (2015).

[37] G. Xing, L. Shang, Y. Fu, W. Ren, X. Fan, W. Zheng, and D. Singh, arXiv:1903.08457 (2019).

[38] M. Sigrist, T. Rice, and F. Zhang, Phys. Rev. B **49**, 12058 (1994).

[39] T. M. Rice, S. Gopalan, and M. Sigrist, Europhysics Letters (EPL) **23**, 445 (1993).

[40] S. Calder, K. An, R. Boehler, C. Dela Cruz, M. Frontzek, M. Guthrie, B. Haberl, A. Huq, S. A. Kimber, J. Liu, *et al.*, Review of Scientific Instruments **89**, 092701 (2018).

[41] M. T. McDonnell, D. P. Olds, K. L. Page, J. C. Neufeind, M. G. Tucker, J. C. Bilheux, W. Zhou, and P. F. Peterson, Acta Crystallogr. Sect. A **73**, a377 (2017).

[42] J. Neuefeind, M. Feygenson, J. Carruth, R. Hoffmann, and K. K. Chipley, Nucl. Instrum. Methods **287**, 68 (2012).

[43] See Supplemental Material at [] for details pertaining to: sample synthesis, diffraction data collection, Rietveld refinements and a more indepth discussion of the DFT results.

[44] J. Rodríguez-Carvajal, Physica B: Condensed Matter **192**, 55 (1993).

[45] A. Larson and R. Von Dreele, Los Alamos National Laboratory, Los Alamos, NM Report No. LAUR , 86 (2004).

[46] R. B. Von Dreele, J. D. Jorgensen, and C. G. Windsor, Journal of Applied Crystallography **15**, 581 (1982).

[47] L. W. Finger, D. E. Cox, and A. P. Jephcoat, J. Appl. Cryst. **27**, 892 (1994).

[48] G. Kresse and D. Joubert, Phys. Rev. B **59**, 1758 (1999).

[49] G. Kresse and J. Furthmüller, Phys. Rev. B **54**, 11169 (1996).

[50] J. P. Perdew, K. Burke, and M. Ernzerhof, Phys. Rev. Lett. **77**, 3865 (1996).

[51] D. Singh and L. Nordström, *Planewaves, Pseudopotentials and the LAPW Method*, $2^{nd}$ ed. ed. (Springer, Berlin, 2006).

[52] P. Blaha, K. Schwarz, G. Madsen, D. Kvasnicka, and J. Luitz, *WIEN2k, An augmented plane wave + lcal orbitals program for calculating crystal properties* (2001).

[53] A. Togo and I. Tanaka, Scr. Mater. **108**, 1 (2015).

[54] A. Subedi, Phys. Rev. B **92**, 174501 (2015).

[55] T. Forrest, P. Valdivia, C. Rotundu, E. Bourret-Courchesne, and R. Birgeneau, Journal of Physics: Condensed Matter **28**, 115702 (2016).

[56] G. Becht, J. Vaughey, R. Britt, C. Eagle, and S.-J. Hwu, Materials Research Bulletin **43**, 3389 (2008).

[57] V. Sears, Neutron News **3**, 26 (2006).

[58] L. Temleitner, A. Stunault, G. Cuello, and L. Pusztai, Phys. Rev. B **92**, 014201 (2015).

[59] M. Gupta, R. Gupta, and D. Singh, Phys. Rev. Lett. **95**, 056403 (2005).

[60] H. Khan and C. Raub, Journal of the Less Common Metals **49**, 399 (1976).

[61] Y. Feng, X.-W. Zhang, Y.-Q. Hao, A. D. Hillier, D. T. Adroja, and J. Zhao, Phys. Rev. B **99**, 174401 (2019).

[62] J. Rowe, J. Rush, H. Smith, M. Mostoller, and H. Flotow, Phys. Rev. Lett. **33**, 1297 (1974).

[63] A. Aguayo, I. Mazin, and D. Singh, Phys. Rev. Lett. **92**, 147201 (2004).

[64] J.-J. Xiang, Y.-L. Yu, S.-Q. Wu, B.-Z. Li, Y.-T. Shao, Z.-T. Tang, J.-K. Bao, and G.-H. Cao, Phys. Rev. Materials **3**, 114802 (2019).